Rheo-optical studies of carbon nanotube suspensions

D. Fry and B. Langhorst
National Institute of Standards and Technology, Gaithersburg, Maryland 20899

H. Wang
Department of Materials Science and Engineering, Michigan Technological University, Houghton, Michigan 49931

M. L. Becker and B. J. Bauer
National Institute of Standards and Technology, Gaithersburg, Maryland 20899

E. A. Grulke
Department of Chemical Engineering, University of Kentucky, Lexington, Kentucky 40506

E. K. Hobbie[a)]
National Institute of Standards and Technology, Gaithersburg, Maryland 20899

(Received 9 August 2005; accepted 29 November 2005; published online 1 February 2006)

We use a polarization-modulation technique to investigate the optical anisotropy of multi- and single-wall carbon nanotubes suspended in a variety of solvents under simple shear flow. Measurements of birefringence and dichroism are performed as a function of shear rate, tube concentration, and solvent viscosity. At fixed volume fraction, the anisotropy increases with increasing shear stress due to enhanced flow alignment. At fixed shear stress, the anisotropy increases with volume fraction due to rotational excluded-volume interactions. By considering the rotational diffusivity as a function of nanotube length, diameter, concentration, and solvent viscosity, we demonstrate a leading-order scaling relation for the optical anisotropy in terms of rotary Peclet number Pe. At low Pe, our results are in qualitative agreement with the theoretical predictions of Doi and Edwards. At high Pe, our data suggest that the degree of nanotube alignment scales as $Pe^{1/6}$. © *2006 American Institute of Physics*. [DOI: 10.1063/1.2159488]

I. INTRODUCTION

Carbon nanotubes hold remarkable promise for next generation materials, with potential applications in organic electronics, reinforced and electrically conducting plastic composites, new alloys, and even new types of biological sensors and devices.[1] Efficient bulk processing schemes yielding highly purified samples that are relatively monodisperse in length, diameter, and electrical properties do not yet exist, however, creating the primary bottleneck to the development of new carbon-nanotube-based materials at commercial production scales. To a significant extent, overcoming this bottleneck will require a detailed understanding of the dependence of material properties on the variables that limit and control flow processing, such as composition, temperature, aspect ratio, and shear stress. Tools that directly measure and characterize carbon nanotube dispersion, stability, and alignment have so far been mostly limited to the various conventional scattering techniques, such as small-angle light scattering (SALS), small-angle neutron scattering (SANS), and small-angle x-ray scattering (SAXS),[2–4] each with its own unique ability to probe different regimes of nanotube length and diameter. It is reasonable to suggest that future progress will rely heavily on the development of new measurement techniques, as well as the adaptation of existing metrologies, specifically designed to probe the nonequilibrium structure and dynamics of soft carbon-nanotube-based materials.

Here, we report what to our knowledge is one of the first optical studies to measure the birefringence and dichroism of flowing carbon nanotube suspensions. We use a polarization-modulation technique to investigate the anisotropy of multi- and single-wall carbon nanotubes suspended in a variety of solvents. What makes the rheo-optical technique particularly useful is the inherently biased selection of shape anisotropy. A tremendous problem of considerable practical importance is carbon nanotube purification. Large, relatively shape symmetric aggregates of carbon nanotubes, which are known to form under many processing conditions, are not birefringent or dichroic and thus will not contribute to the signal measured using this method. Measurements of the optical anisotropy are performed as a function of shear rate, tube concentration, and solvent viscosity. At fixed nanotube volume fraction, the anisotropy increases with increasing shear stress due to enhanced flow alignment. At fixed shear stress, the anisotropy increases with volume fraction due to excluded-volume interactions. By considering the rotational diffusivity as a function of tube length, diameter, concentration, and solvent viscosity, we demonstrate a leading-order scaling relation in terms of rotary Peclet number Pe. At low to modest Pe, our results are in qualitative agreement with the theoretical predictions of Doi and Edwards. In the limit of large-to-infinite Pe, our data suggest that the degree of nanotube

[a)]Electronic mail: erik.hobbie@nist.gov

alignment grows in a power-law fashion as $Pe^{1/6}$. Our goal here is to investigate the feasibility of rheo-optical techniques for measuring and quantifying dispersion and orientation in flowing carbon nanotube suspensions. In particular, we measure the degree of flow-induced optical anisotropy and its dependence on shear stress, tube dynamics, and carbon nanotube concentration. The effectiveness of simple shear flow for aligning carbon nanotubes in the dilute and semidilute regimes is found to be limited by the magnitude of the rotational Peclet number, which has profound implications for the use of simple shearing flows for orienting carbon nanotubes in soft materials.

II. EXPERIMENTAL SETUP

A. Sample preparation

The multi-wall carbon nanotubes (MWCNTs) were grown via chemical-vapor deposition (CVD) and suspended in low-molecular-mass polyisobutylene (PIB) fluids using polymer dispersant as described previously.[5] The mean diameter is $d \approx 50$ nm and the mean length is $L \approx 10$ μm ($L/d \approx 200$) as determined by electron and optical microscopies, respectively. The size distribution is nearly log normal with an approximate polydispersity index of 2. The MWCNTs were suspended in two different media, with the final suspensions denoted by M1 and M2. M1 was prepared by adding toluene-dispersed MWCNTs at various concentrations to a PIB Boger fluid, made by mixing 0.1% by mass $M_w = 4.7 \times 10^6$ PIB with $M_w = 800$ PIB. The resulting fluid is viscoelastic with a constant shear viscosity of $\eta_s \approx 10$ Pa s and a first normal stress difference $N_1 \approx 3.68\dot{\gamma}^{2.38}$ (Pa) over the interval $1\ s^{-1} < \dot{\gamma} < 10\ s^{-1}$, where $\dot{\gamma}$ is the shear rate. No flow instability was apparent in the pure PIB Boger fluid over the range of shear rates of interest here. The second sample, denoted as M2, was similarly prepared in a Newtonian PIB fluid of $M_w = 500$ and $\eta_s = 0.5$ Pa s. All samples were mixed in toluene, stirred slowly for several days until homogeneous, and then placed in a vacuum oven for approximately 48 h to remove the toluene. For M1, suspensions were prepared at 0.1%–0.8% MWCNT by mass, with $cL^3 \approx 24-200$, where c is the number of tubes per unit volume. For M2, suspensions were prepared at 0.025%–0.85% MWCNT by mass, with $cL^3 \approx 6-210$. For both M1 and M2, the shear viscosity η is comparable to the solvent viscosity η_s when the nanotubes are well dispersed and $cL^2d < 1$. Although the MWCNTs are coated with a polymeric dispersant,[5] the tube-tube interactions are weakly attractive and the MWCNTs in M1 and M2 slowly aggregate, both in quiescence and under weak shear. The clustering in quiescence is limited in scale, but the clusters coarsen considerably in weak shear over the course of several minutes to several hours.[5] Our results suggest that the stability limit for MWCNT dispersion in M1 and M2 occurs at a shear stress of roughly 5 Pa, with matrix elasticity having a negligible effect. This critical stress is dictated by the strength of the contact potential and the coefficient of static friction between contacted nanotubes. Samples of interest here were homogenized at high shear rate and subjected to a damped oscillatory shear flow prior to performing measurements at each shear rate.

Single-walled carbon nanotubes (SWCNTs) synthesized via the high-pressure catalytic decomposition of carbon monoxide (HiPCO) were obtained commercially in dry powder form from CNI, Inc.[6] Two different suspending fluids were used in this study: an aqueous ionic surfactant solution[7] and an aqueous single-stranded DNA (ssDNA) solution.[8] Resulting samples are denoted S1 and S2, respectively. The surfactant suspension S1 was prepared by mixing 0.6% by mass fraction sodium dodecylbenzenesulfonate (NaDDBS) in 99.96 at. % isotopic purity D_2O. The resulting solution had a shear-independent viscosity of 9.5×10^{-4} Pa s. After addition of the SWCNTs (purified through thermal oxidation at 260 °C, refluxed in HCl solution, and ultrasonicated in nitric acid) the sample was sonicated in an ice bath for 10 h. The resulting suspension contained bundles of individual SWCNTs. Atomic force microscopy (AFM) analysis of dried films gave a mean bundle diameter $d \approx 13.5$ nm and a mean length $L \approx 0.75$ μm ($L/d \approx 60$). We focus on 0.08%–0.15% SWCNT by mass, with $cL^3 \approx 1.7-3.3$ and $cL^2d < 1$.

The second sample S2 was made by suspending SWCNTs in an aqueous ssDNA solution. The DNA consisted of 30 guanine/thiamine (G/T) base pairs with $M_w = 9.44 \times 10^3$ and was obtained from Integrated DNA Technologies, Inc.[9] The as-received DNA sample was dry and had been prepared with standard desalting techniques. It was rehydrated in a 0.1 mol/L $NaCl/D_2O$ stock solution at 1 mg/mL and allowed to rest for 12 h. The SWCNTs were then added in dry form with no prior purification at 1 mg/mL and sonicated at 3 W in an ice bath for 90 min, at which point the solution was black and completely opaque in a 1 mL couvette. Further purification was achieved through centrifugation at 15 000 g for 90 min. As in S1, the tubes in the aqueous ssDNA solution exist as bundles, with AFM giving the average $d \approx 5$ nm and a mean length $L \approx 0.50$ μm ($L/d \approx 100$) after centrifugation. Although AFM measurements were not performed on the initial (uncentrifuged) suspensions, it is reasonable to assume that they are comparable in particle size to the suspensions prepared with the ionic surfactant NaDDBS, with $d \approx 10$ nm and a mean length $L \approx 0.50-0.70$ μm ($L/d \approx 60$). We focus on an initial concentration of 0.1% SWCNT by mass, with $cL^3 \approx 2$ and $cL^2d < 1$. As described below, we obtain a rescaled concentration for the centrifuged samples via UV-visible (UV-VIS) absorption measurements. The shear viscosity of the ssDNA-dispersed SWCNT suspensions is again comparable to that of water. The aqueous SWCNT suspensions S1 and S2 are stable, both in quiesence at all shear rates of interest here.

B. Rheo-optical technique

The birefringence and dichroism were measured as a function of shear rate utilizing a polarization-modulation lock-in technique.[10] The apparatus consists of a Rheometric Scientific SR-5000 stress-controlled rheometer equipped with an optical train supplied by Rheometric.[11,12] The optical shear cell is made with two polished quartz plates of 40 mm nominal outer diameter and is constructed such that the plate normal is parallel to the quartz optical axis, eliminating any

contribution of residual birefringence from the quartz. We consider linear shear flow along $\hat{\mathbf{x}}$, a constant velocity gradient along $\hat{\mathbf{y}}$, and vorticity along $\hat{\mathbf{z}}$, with

$$\dot{\gamma} = \partial v_x / \partial y. \tag{1}$$

The incident wave vector $\mathbf{k}_i = k_i \hat{\mathbf{y}}$ is normal to the sample cell plate (parallel to the velocity gradient direction), restricting our measurements of optical anisotropy to the flow-vorticity plane.

The technique we use is similar to that used in a large number of past studies of polymeric and colloidal systems.[10,13,14] The optical assembly consists of a 8 mW diode laser of wavelength $\lambda = 670$ nm, a half-wave plate rotating at angular frequency $\Omega = 400$ Hz, a beam splitting cube, and a 90° deflector and two solid-state photodiode detectors for recording the incident and transmitted light intensity. Light exiting the laser is linearly polarized. It passes through the half-wave plate where its polarization state is modulated at frequency Ω. The beam is then split into two signals, one providing the reference signal for phase locking and the other passing through the sample. The incident beam strikes the sample 18.5 mm from the center of the sample cell with a beam diameter of 1.5 mm. The active sample detector area is 16 mm^2.

Both the reference and transmitted signals from the photodiode are sent to the lock-in amplifier which demodulates the transmitted signal by Fourier decomposition. Once demodulated, $\Delta n'$ and $\Delta n''$ are calculated according to

$$\delta' = \frac{2\pi \ell \Delta n'}{\lambda}, \qquad \delta'' = \frac{2\pi \ell \Delta n''}{\lambda}, \tag{2}$$

where δ' is the difference in phase between the reference and transmitted signals, δ'' is the attenuation of light intensity, and ℓ is the sample thickness, defined here by the gap between the plates. It is important to note that the signal-to-noise ratio will be inherently larger for the dichroism, which depends on the ratio of measured intensities. In contrast, the birefringence is obtained from a simple phase shift, which is relatively easy to measure precisely with the lock-in technique. Optical calibration was performed using a quartz zero-order quarter-wave plate with a uniaxial birefringence $\Delta n' = 9.03 \times 10^{-3}$ at $\lambda = 670$ nm (Ref. 15) and a linear dichroic sheet polarizer with a $1:10^4$ extinction ratio, respectively. All calibration measurements matched the expected values to within 1%. For M1 and M2, we restrict our measurements to shear rates where the suspensions are homogeneous and the tubes dispersed.[5]

Considering the simple picture of nanotubes as rigid nanoscale fibers or rods, we expect that the optical anisotropy will depend on nanotube mobility, aspect ratio, and concentration, as well as the shear rate $\dot{\gamma}$. The dilute and semidilute regimes are delineated according to[16]

$$cL^2 d < 1, \quad cL^3 < 1 \text{ dilute}, \qquad cL^2 d < 1, \quad cL^3 > 1 \text{ semidilute}, \tag{3}$$

where c is the number density of nanotubes. Based on the values of cL^3 and $cL^2 d$ quoted above in Sec. II A for M1, M2, S1, and S2, we see that our rodlike suspensions span the transition from dilute to semidilute.

The Reynolds number Re for the parallel plate geometry used here can be defined as

$$\mathrm{Re} = \frac{\rho_s \dot{\gamma} \ell^2}{\eta_s}, \tag{4}$$

where ρ_s and η_s are the solvent density and viscosity, respectively, and ℓ is the gap of the cell. For M1 and M2, Re is less than 0.05. In S1 and S2, which have a much lower solvent viscosity, Re reaches a maximum value of roughly 1000 for 0.1% S1 at 4000 s^{-1}, but is more typically less than 300. We note that turbulent flow effects do not usually emerge until Re is of order 2000 or larger.

All measurements were performed at 25 °C, with each shear rate averaged for 4 min at a sampling time of 2 s/pt. This was repeated 3–5 times for each sample and in some cases for different sample loadings on different days. The largest source of error was found to be due to fluctuations at fixed shear during a single measurement, with the largest being for the MWCNT samples (ca. 8%). Run-to-run reproducibility in values of both birefringence and dichroism was good. Sample thickness, limited by low light transmittance at the highest concentrations, was 100–200 μm (M1 and M2) and 600 μm (S1 and S2). The smallest thickness was still an order of magnitude larger than the largest mean tube length. All listed errors and error bars represent an uncertainty of two standard deviations.

Figure 1(a) shows the response of the neat PIB Boger fluid. The measured optical response for air is also shown (inset). Note that the birefringence of the quartz plates is zero, as previously noted (Sec. II B). As expected, the optical response of the pure solution is essentially zero at $\lambda = 670$ nm. Results for the pure NaDDBS solution are shown in Fig. 1(b). The dichroism (not shown) was also found to be approximately zero. The pure ssDNA solution gave similar results. The measured birefringence and dichroism of all multiwalled and single-walled carbon nanotube suspensions were found to be 1–3 orders of magnitude larger than these background signals, and any contribution from solvents is thus neglected.

III. RESULTS AND DISCUSSION

A. MWCNTs

The shear-induced birefringence and dichroism for M1 and M2 as a function of $\dot{\gamma}$ are shown in Fig. 2. For all samples, $\Delta n'$ and $\Delta n''$ show a modest increase with increasing shear rate due to an increased degree of alignment along the flow direction, and a dramatic increase with volume fraction. In the limit of perfectly aligned rigid rods, both the birefringence and dichroism would be maximum, defining the intrinsic anisotropy in nanotube permittivity. Conversely, these would be zero for a random or isotropic orientation. The tubes are in any one of a family of closed periodic "Jef-

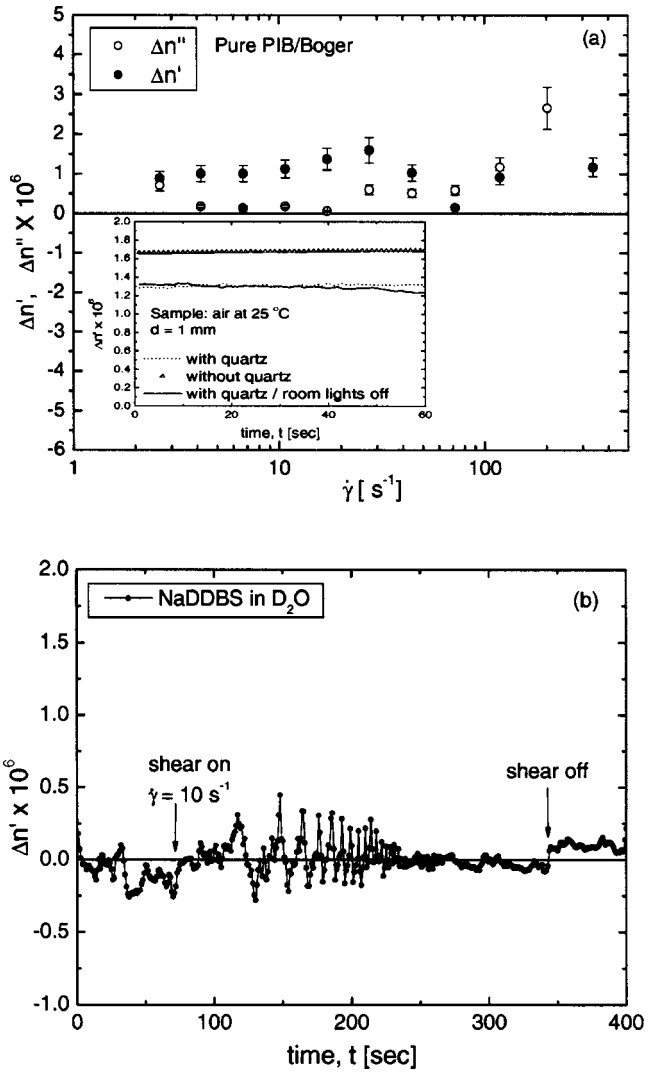

FIG. 1. The background birefringence and dichroism as a function of shear rate for both (a) a pure PIB/Boger fluid and (b) an aqueous NaDDBS solution. Results for the pure 500 MW PIB and aqueous ssDNA solutions were similar in the magnitude of the measured background anisotropy. For comparison we also show results for an empty sample cell, i.e., nothing but air, with and without the quartz sample plates.

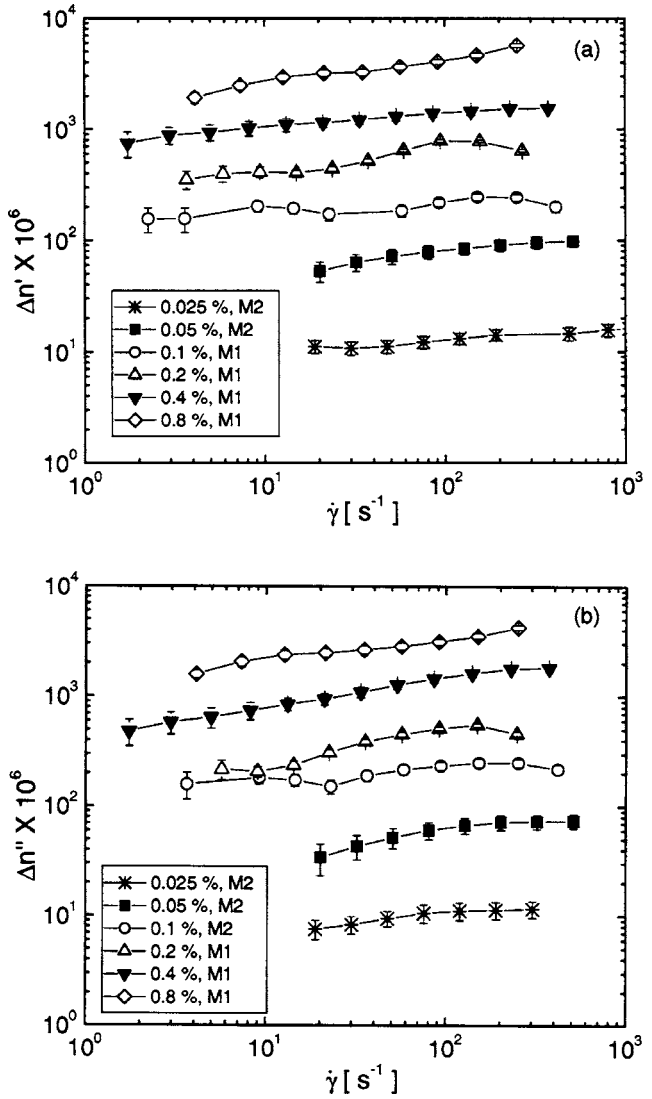

FIG. 2. Birefringence (a) and dichroism (b) as a function of shear rate for M1 and M2. All concentrations are denoted in percent mass fraction.

fery" orbits about the vorticity axis, rotating with a period that depends on L/d and $\dot{\gamma}$.[16,17] Although the distribution of orbits is set by tube interactions,[17] at any given instant, the ensemble contains a number of orientations, and our measurements capture an average over this ensemble.

An extensive amount of work has been done on the flow birefringence of polymeric systems and colloidal dispersions.[13,14] When dilute, polymeric and colloidal systems are weakly birefringent at modest shear rates ($\lesssim 100\ s^{-1}$) with magnitudes of ca. $\Delta n' \lesssim 10^{-6}$.[13,18] However, for liquid-crystalline polymers[19] and common crystals such as calcite and quartz, $\Delta n'$ is typically greater than 10^{-3} and even as large as 10^{-1}. Our results show that depending on tube concentration, $10^{-5} < \Delta n' < 9 \times 10^{-2}$, an order of magnitude larger than that of dilute polymeric and colloidal systems and comparable to that of common birefringent crystals. Note that by symmetry, the nanotubes are, intrinsically, uniaxially birefringent, as is the case for quartz. Here we assume, for the case of simplicity, that the symmetry of the orientational distribution function (ODF) of the nanotube suspension is likewise uniaxial, although in reality it likely exhibits a degree of asymmetry when projected into the gradient-vorticity plane.[17]

To understand how the bulk optical anisotropy depends on nanotube concentration and flow, we first rescale $\Delta n'$ and $\Delta n''$ by ϕ, leaving only the optical anisotropy and the (effective) nematic order parameter.[20] M1 and M2 consist of multiwalled tubes suspended in solvents of different molecular weight and hence different shear viscosity. To proceed further, we make cuts in $\Delta n'/\phi$ and $\Delta n''/\phi$ versus shear stress τ at fixed $\tau = 50$, 100, and 200 Pa. Results (see Fig. 3) for each τ are relatively closely spaced and appear to fall on a common curve. A linear regression on a log-log plot yields an exponent $\mu = 0.3 \pm 0.05$, implying that $\Delta n'$ and $\Delta n''$ scale approximately as $\phi^{4/3}$.

We also note the rather large inherent dichroism of the multiwalled carbon nanotube suspensions. All multiwalled samples were black in color with very low light transmission. MWCNTs and SWCNTs are known to absorb quite strongly from the ultraviolet to the near infrared,[21–24] reflect-

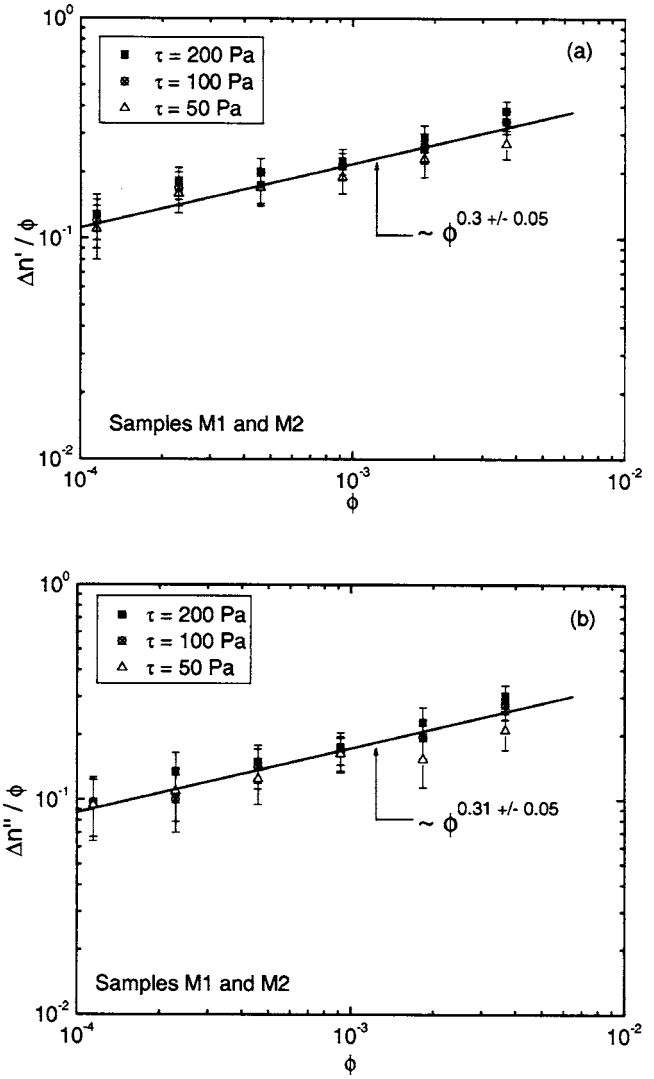

FIG. 3. Volume-fraction normalized birefringence (a) and dichroism (b) as a function of ϕ for samples M1 and M2. All data correspond to a fixed shear stress τ. All concentrations are denoted in percent by mass.

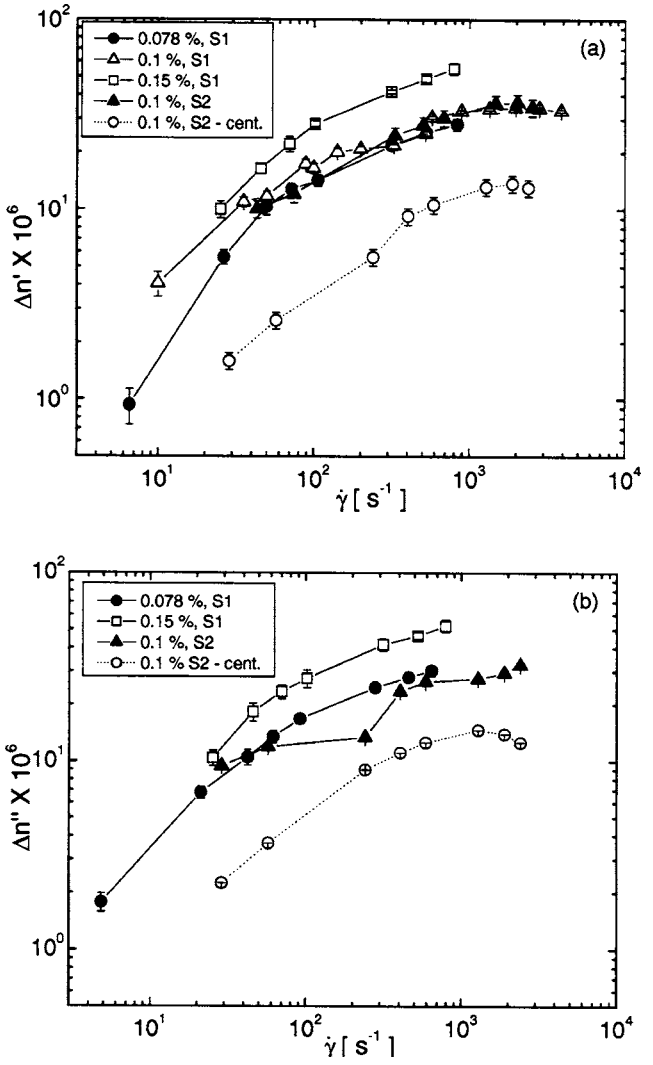

FIG. 4. Birefringence (a) and dichroism (b) as a function of shear rate for samples S1 and S2. All concentrations are denoted in percent by mass. In the case of 0.1% S2 after centrifugation, a comparison of optical absorption spectra for the two S2 suspensions (Fig. 5) shows that the corrected volume fraction is a factor of 2.4 smaller than that before centrifugation.

ing a significant imaginary component to the complex index of refraction tensor. Given the unique anisotropic structure of the nanotubes and hence the intrinsic anisotropy in electron mobility, it is not surprising that they are strongly dichroic.

B. SWCNTs

Shear-induced birefringence and dichroism for the SWCNT samples S1 and S2 are shown in Fig. 4. Like the MWCNT samples, $\Delta n'$ and $\Delta n''$ increase with shear rate. However, both are more than a factor of 10 smaller in magnitude than in M1 and M2. A derivation of the complex dielectric tensor of nanotube suspensions to second order in fluctuations is presented elsewhere.[20] The intrinsic optical anisotropy depends on free and bound charge mobilities, which is inherently different along and normal to the nanotube axis. Moreover, defects, present to some degree in all nanotubes, will strongly influence charge mobility. Due to both inherent structure and the methods by which they are grown, multiwalled tubes typically have a larger number of defects compared to single-walled tubes, with electron transport being diffusive rather than ballistic.[25,26] The usual expression for the dichroism and the birefringence gives $\Delta n'$ and $\Delta n''$ in terms of the nanotube volume fraction, the (mean) intrinsic optical anisotropy of an individual tube, and a (para)nematic order parameter dictated by the ODF. Specifically, we obtain[20]

$$n_{\parallel} \approx n_s + (\phi/2n_s)[(\alpha_{\parallel} - \alpha_{\perp})\psi + (\alpha_{\perp} - \epsilon_s)] + \cdots \tag{5}$$

and

$$n_{\perp} \approx n_s + (\phi/2n_s)[(\alpha_{\parallel} - \alpha_{\perp})(1 - \psi)/2 + (\alpha_{\perp} - \epsilon_s)] + \cdots \tag{6}$$

for the complex indices of refraction along and normal to the direction of mean alignment, respectively. In these equations, n_s and ϵ_s are the index of refraction and dielectric constant of the solvent, $\alpha_{\parallel} = \alpha'_{\parallel} + i\alpha''_{\parallel}$ and $\alpha_{\perp} = \alpha'_{\perp} + i\alpha''_{\perp}$ are the complex permittivities along and normal to a nanotube axis, ϕ is the volume fraction of nanotubes, and $\psi = \langle \cos^2(\theta) \rangle$, where θ is the angle a nanotube makes with the direction of mean align-

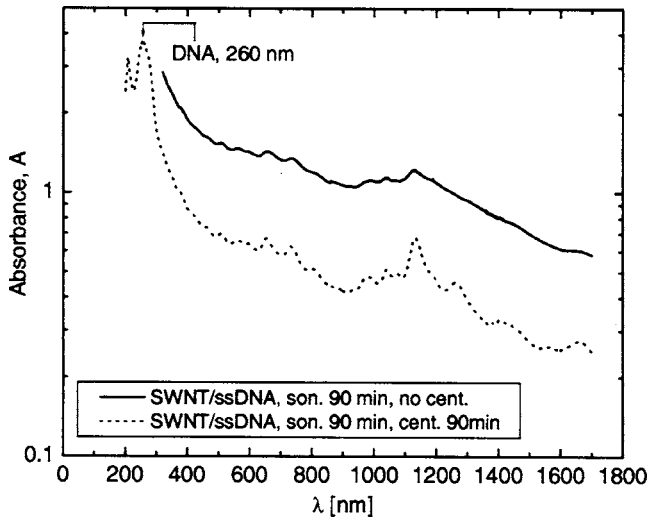

FIG. 5. Absorption spectrum for sample S2 (0.1% by mass) before and after centrifugation for 90 min at 15 000 g. The DNA peak at ≈260 nm is clearly visible. Note the decrease in absorbtion and the increase in peak resolution after centrifugation.

ment and the brackets denote an average over the ODF. The birefringence is thus $\Delta n' \approx (\alpha'_\perp - \alpha'_\perp) S\phi/(2n_s)$ and the dichroism is $\Delta n'' \approx (\alpha''_\parallel - \alpha''_\perp) S\phi/(2n_s)$, where $S = \langle P_2(\cos\theta)\rangle = \frac{1}{2}[3\langle\psi\rangle - 1]$ is a nematic order parameter, being zero for an isotropic distribution and 1 for perfect alignment. By combining a variety of experimental techniques, we have found that the degree of alignment for the SWCNT suspensions S1 and S2 is considerably smaller than that for the M1 and M2, reflecting their dilute nature and the smaller value of L/d.[27] By taking this into account, we have shown that the SWCNTs have a larger intrinsic optical anisotropy, consistent with fewer defects and a higher degree of purity.[27] Specifically, we find $\alpha'_\parallel - \alpha'_\perp \approx 1.95$ and $\alpha''_\parallel - \alpha''_\perp \approx 2.15$ for the SWCNTs and $\alpha'_\parallel - \alpha'_\perp \approx 1.65$ and $\alpha''_\parallel - \alpha''_\perp \approx 1.28$ for the MWCNTs at $\lambda = 670$ nm.

Recent studies suggest that ssDNA is an effective dispersant for SWCNTs and SWCNT bundles in aqueous solution.[8] In particular, centrifuging such suspensions resulted in a better degree of dispersion, measured in part by UV/VIS/near infrared (NIR) spectroscopy. Because of their reduced length, individual nanotubes in general will have a greater rotational mobility than SWCNT bundles, and hence at any given shear rate a reduced anisotropy. Rheo-optical results for the centrifuged SWCNT/ssDNA sample (S2, centrifuged) are also shown in Fig. 4. There is a reduction in optical anisotropy over the entire range of shear rate. However, the change appears to be in part multiplicative in magnitude by a factor of ca. 2.5±0.3, implying a substantial change in overall nanotube concentration due to the removal of mass. As a consistency check we have also performed UV/VIS/NIR spectroscopy on the SWCNT/ssDNA samples (see Fig. 5). The MWCNT samples were too concentrated to perform similar measurements. Measurements were taken with a Perkin-Elmer Lambda 9 UV/VIS/NIR spectrophotometer,[12] capable of scanning wavelengths from 200–1600 nm. After centrifugation, the absorption peaks become moderately sharper and roughly agree with previous measurements.[8] But, more importantly, the magnitude also appears to decrease by a constant factor, ca. ≈2.4, providing a quantitative measure of the reduction in overall mass.

C. Universal scaling

As discussed above, neither $\Delta n'$ nor $\Delta n''$ appear to scale in an exclusively linear fashion with volume fraction for M1 and M2, implying that the simplified view of negligible interactions between nanotubes does not apply in the semidilute regime. We now show that one can account for this by including the effects of excluded-volume interactions. In the dilute limit, the thermal rotary diffusion coefficient for rigid Brownian rods is[16,28]

$$D_r = D_o = 3k_BT[\ln(L/d) - 0.8]/(\pi\eta L^3). \tag{7}$$

This simple expression should have some validity for the SWCNT samples (S1 and S2), which are Brownian and sufficiently dilute with $cL^3 \approx O(1)$, but not for the semidilute MWCNT suspensions, for which cL^3 is significantly larger than unity, implying overlap in the excluded volume swept out by rotating nanotubes. In the semidilute regime, we thus need to use an appropriately rescaled expression for the rotational diffusivity that explicitly includes excluded-volume effects,[16,28]

$$D_r = \beta D_o (cL^3)^{-2} \propto D_o \phi^{-2}, \tag{8}$$

where $\beta \approx 1350$.[16] There will be higher-order corrections to Eq. (8) associated with structural anisotropy in flow-aligned suspensions[16,28] that we ignore here as a first approximation. Figure 6 shows the scaled birefringence and dichroism as a function of rotational Peclet number $\mathrm{Pe} = \dot\gamma/D_r$. For S1 and S2, which are both dilute, we have used Eq. (7), while for M1 and M2 we have used Eq. (8). The data roughly scale over 10 decades in Pe without any free parameters, falling into two distinct groups by nanotube type and L/d. For the MWCNT data, $\Delta n/\phi \propto \mathrm{Pe}^{0.16}$ suggests a weak power-law dependence for the degree of flow-induced alignment in the limit of very large Pe.

From an order-of-magnitude perspective, the overlap in Fig. 6 is admittedly striking, but one might question the appropriateness of Eqs. (7) and (8) for M1 and M2. Depending on the magnitude of Pe, the MWCNT samples range from marginally Brownian to very non-Brownian, and it can be argued that a temperature-dependent rotary diffusion coefficient is not immediately relevant. Koch has proposed[29] that the rotary diffusion coefficient for non-Brownian semidilute fiber suspensions under simple linear shear flow is given by

$$D_r \propto cL^3\dot\gamma, \tag{9}$$

where the constant of proportionality scales inversely with $(L/d)[\ln(L/d)]^2$. Inherent to the model is that rotary diffusion in non-Brownian suspensions is predominantly hydrodynamic in nature. Rotary motion is induced when neighboring fibers are swept into the vicinity of a test fiber by the imposed flow field. For our purposes we need to form a dimensionless group, analogous to the Brownian Peclet number defined above in its volume fraction and shear rate dependence. To do so, we heuristically reduce D_r by

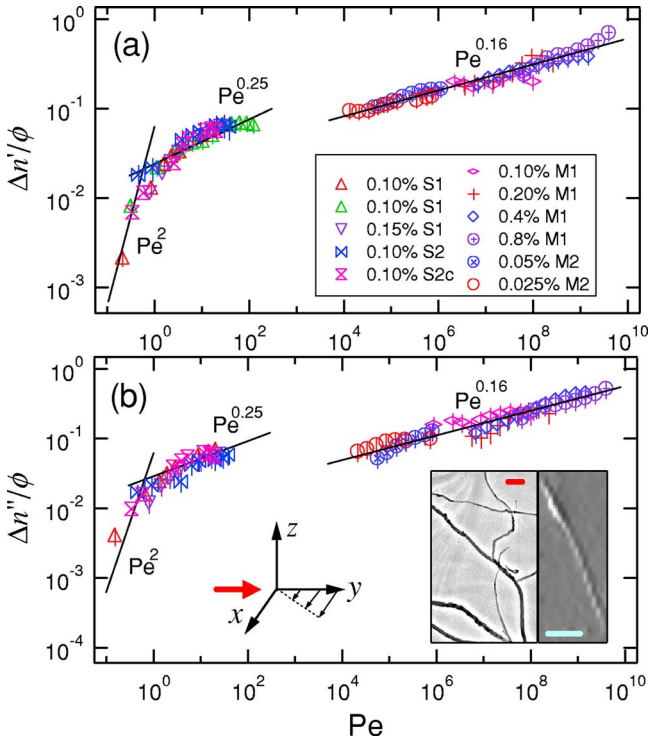

FIG. 6. (Color online). Scaled birefringence (a) and dichroism (b) as a function of Peclet number. The data break naturally into two groups; single wall and multiwall. The solid lines represent power-law fits with exponents as indicated. The lower left inset shows a post-dispersion electron micrograph of the MWCNTs (scale bar=250 nm) and the lower right inset is an AFM image of a SWCNT bundle (scale bar=150 nm). The geometry of the flow and the optical measurement are also depicted. The volume fraction of 0.1% S2 was determined from UV-VIS absorption (Fig. 5). For all of the samples except 0.1% S2, there are no unknown parameters in this scaling plot. For 0.1% S2, we have assumed $d \approx 10$ nm and $L \approx 0.60$ μm.

$$\tau = (\tau_o/\eta_s)(\eta - \eta_s), \tag{10}$$

which vanishes for $\phi \to 0$, with τ_o being any dilute relaxation time (e.g., D_o^{-1} for the thermal rotation of Brownian tubes). Appropriately, the *generalized* Peclet number

$$D_r\tau \propto cL^3\dot{\gamma}\tau_o[\eta]\phi \propto \dot{\gamma}\tau_o[\eta]\phi^2, \tag{11}$$

where $[\eta]$ is the intrinsic viscosity, has the same $\dot{\gamma}$ and ϕ^2 scaling as derived above, consistent with the behavior in Fig. 6. This expression gives one the freedom to define an appropriate dimensionless group based on any choice of "bare" time scale in Eq. (10). For example, taking τ_o to be the characteristic relaxation time associated with the elastic deformation of an isolated nanotube would give the same scaling as in Fig. 6, but with the scale of the horizontal axis shifted down by several orders of magnitude.

One might also argue, however, that Brownian diffusion—although extremely slow—is still the appropriate time scale to consider, with the very large values of Pe for M1 and M2 simply giving information relevant to the limit of infinite thermal rotational Peclet number. Such a view might be practical with respect to evaluating the effectiveness of simple shear flow for aligning carbon nanotubes dispersed in viscoelastic polymer melts. Indeed, by conventional polymer standards the M1 and M2 solvent viscosities are small, and a degree of diffusion, although limited and likely intimately linked to other more subtle effects such as slow sedimentation and attractive tube-tube interactions, is detectable over the course of many minutes to several hours in these suspensions. From this perspective, the results shown in Fig. 6 are qualitatively useful, since they provide a guide for predicting the extent of shear-induced alignment in polymer carbon nanotube melt composites. Optical measurements reported elsewhere[27] suggest that the (para)nematic order parameter in M1 and M2 is less than 0.8 at high Pe, and it is presumed that higher solvent viscosities at comparable strain rates would give a degree of improved alignment that could be extrapolated from the weak power-law dependence suggested by the data in Fig. 6.

For the sake of rigor, it is instructive to compare the explicit form of the two different dimensionless groups for the specific case of Brownian rods. In the semidilute regime, the exact thermal rotational Peclet number that follows from Eq. (8) is

$$(4/\pi)^2(\beta D_o)^{-1}(L/d)^4\dot{\gamma}\phi^2, \tag{12}$$

while the heuristic form obtained from Eq. (11) for $\tau_o = D_o^{-1}$ is

$$(4/\pi)^2(\beta_r D_o)^{-1}(L/d)^4\dot{\gamma}\phi^2, \tag{13}$$

where

$$\beta_r \propto (45/2\pi)(L/d)[\ln(L/d)]^2 \ln(2L/d), \tag{14}$$

and we have used the leading-order Kirkwood-Batchelor expression for the intrinsic viscosity of Brownian rigid-rod suspensions.[30] The discrepancy β_r/β, which depends on the aspect ratio L/d, is not all that surprising, since our generalized expression was derived on purely heuristic and dimensional grounds. Our qualitative scaling argument captures the correct volume fraction dependence, however, because the nanotubes still move in a *cage* created by their nearest neighbors regardless of the source of the motion.

As noted above, tube deformation may be an important factor in the shear response, particularly in viscous solvents at exceedingly high Peclet numbers. Although the TEM images in Fig. 6 suggest that the MWCNTs can undergo significant deformation—and can thus deviate from the idealized model of rigid rods—such effects are somewhat artificially enhanced by the TEM grid. A better sense of the *in situ* deformation of MWCNTs in M1 and M2 can be obtained from video micrographs of such suspensions under shear, as shown in Fig. 7. The deformation mechanics of comparable MWCNTs have been measured.[31] The Young's modulus ($E_Y \approx 40$ GPa) and bending stiffness ($B = E_Y \pi d^4/2^6 \approx 1.22 \times 10^{-20}$ Nm^2) compared with 7.5 MPa and 8×10^{-12} Nm^2, respectively, for typical organic fibers. For M1, the dimensionless bending stiffness $B/(\eta_s \dot{\gamma} L^4)$ and bending ratio $E_Y[\ln(2r_e) - 1.5]d^4/(2\eta_s\dot{\gamma}L^4)$, where $r_e = 1.24(L/d)/[\ln(L/d)]^{1/2}$, are 4 and 160, respectively, at 0.03 s^{-1}. At 10 s^{-1}, these are 0.012 and 0.48, respectively. For dimensionless bending ratios less than 1, the tubes will start to deform.[32] The deformation evident in Fig. 7, which is typical for M1 and M2, is modest, and light scattering suggests that the tubes scatter essentially as rigid rods up to the highest shear rates in question.[27] At the highest Pe in Fig. 6,

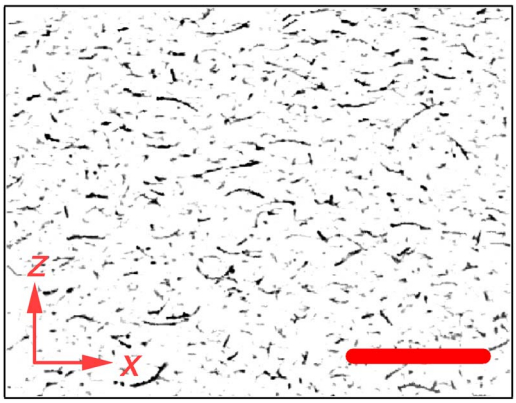

FIG. 7. (Color online). Optical micrograph of 0.5% M1 at a shear rate of 20 s^{-1}. The scale bar is 50 μm, and the flow geometry is as indicated.

however, it is possible that such effects will start to influence the rheology of fiber motion, which in turn will influence quantitative measures of alignment and anisotropy.

IV. CONCLUSIONS

Although solvent elasticity can enhance the flow-induced alignment of isolated fibers,[33] overlay in M1 and M2 suggests a dominance of viscous hydrodynamics in the PIB suspensions of interest here. Doi and Edwards[28] have calculated the degree of alignment S as a function of Peclet number for both dilute and semidilute suspensions of monodisperse rigid rods. In both cases, S scales as Pe^2 in the limit of small Pe, which we show as a power-law fit in Fig. 6. For dilute suspensions at high Pe, the predicted alignment is much stronger than we observe experimentally,[27] perhaps due to polydispersity and tube deformation. Beyond this limit, the computation becomes quite involved due to the presence of tube-tube interactions. For semidilute suspensions at modest Peclet number ($\mathrm{Pe} < 200$), Doi and Edwards predict the leading-order behavior $\mathrm{Pe}^{0.25}$, which we also show over the relevant range of Pe in Fig. 6, in spite of the fact that these suspensions (S1 and S2) are not strictly semidilute, with $cL^3 \approx O(1)$.

Our results are in qualitative agreement with theory. In light of the significant polydispersity and the markedly non-Brownian nature of the MWCNT suspensions, what is perhaps most striking and surprising is the extent to which the effect of excluded-volume interactions can be naively but correctly accounted for in the semidilute regime using the Doi-Edwards expression for thermal rotary diffusion. Without this rescaling, the data for M1 and M2 do not fall onto a master curve. To our knowledge, the limit of infinite Pe has not been studied computationally. Here, our data suggest that $S \propto \phi^{1/3}$, and we hope that this observation will help motivate further theoretical and computational study on such suspensions. Numerical simulations are proving to be an extremely powerful tool for quantifying the rheological behavior of semidilute and semiconcentrated rigid fiber suspensions[34–36] and they will no doubt play a central role in further clarifying experimental observations such as those presented here. It is important to point out that in addition to tube-tube interactions—arising from both hydrodynamics and mechanical contacts—length polydispersity and tube deformation are both likely key factors that would need to be addressed in any effort to explain the large Pe response shown in Fig. 6. At present, carbon nanotubes are inherently polydisperse, due in part to their enormous aspect ratios and small dimensions. We are currently working on fractionating carbon nanotubes by length and future rheo-optical studies will hopefully address the rheological response of such purified suspensions.

Carbon nanotubes hold considerable promise for future technological developments. Progress relies heavily on both the efficient application of current techniques and the development of new measurement methods. We have performed rheo-optical measurements on carbon nanotube suspensions in an attempt to better understand nanotube alignment and dispersion in simple linear shear flow in several systems spanning a broad range of both tube and solvent properties. Much work is still needed, particularly on characterizing dispersive properties of SWCNT suspensions. One avenue of particular interest might perhaps be applying rheo-optical techniques at variable wavelength, particularly at absorption peaks corresponding to intrinsic tube electronic excitation states. This may open up other ways of characterizing the purity of single-walled carbon nanotube suspensions with respect to the conducting (metallic) or semiconducting nature of the tubes. This would be useful for evaluating the suitability of a particular suspension for microelectronic applications.

[1] R. H. Baughman, A. A. Zakhidov, and W. A. de Heer, Science **297**, 287 (2002).
[2] E. K. Hobbie, H. Wang, H. Kim, S. Lin-Gibson, and E. A. Grulke, Phys. Fluids **15**, 1196 (2003).
[3] H. Wang, W. Zhal, D. L. Ho, K. L. Winey, J. E. Fischer, C. J. Glinka, and E. K. Hobbie, Nano Lett. **4**, 1789 (2004).
[4] D. W. Schaefer, J. Zhao, J. M. Brown, D. P. Anderson, and D. W. Tomlin, Chem. Phys. Lett. **375**, 369 (2003); D. W. Schaefer, J. M. Brown, D. P. Anderson, J. Zhao, K. Chokalingam, and D. Tomlin, J. Appl. Crystallogr. **36**, 553 (2003).
[5] S. Lin-Gibson, J. A. Pathak, E. A. Grulke, H. Wang, and E. K. Hobbie, Phys. Rev. Lett. **92**, 048302 (2004).
[6] Carbon Nanotechnologies Incorporated, 16200 Park Row, Houston, TX 77084-5195, Lot No. P0257.
[7] M. F. Islam, E. Rojas, D. M. Bergey, A. T. Johnson, and A. G. Yodh, Nano Lett. **3**, 269 (2003).
[8] M. Zheng, A. Jagota, M. S. Strano *et al.*, Science **302**, 1545 (2003).
[9] Integrated DNA Technologies, Inc., 1710 Commercial Park, Coralville, IA 52241-2760.
[10] G. G. Fuller, *Optical Rheometry of Complex Fluids* (Oxford University Press, New York, 1995).
[11] Rheometric Scientific, Inc., One Possumtown Road, Piscataway, NJ 08854. Currently (2003) TA Instruments, Inc.
[12] Certain commercial materials and equipment are identified in this paper in order to specify adequately the experimental procedure. In no case does such identification imply recommendation by the National Institute of Standards and Technology nor does it imply that the material or equipment identified is necessarily the best available for this purpose.
[13] G. G. Fuller and K. J. Mikkelsen, J. Rheol. **33**, 761 (1989).
[14] P. L. Frattini and G. G. Fuller, J. Rheol. **28**, 61 (1984).
[15] CVI Laser, LLC, 200 Dorado Place SE, Albuquerque, New Mexico 87123.
[16] R. G. Larson, *The Structure and Rheology of Complex Fluids* (Oxford University Press, New York, 1999).
[17] The tubes are in any one of a family of closed periodic Jeffery orbits around $\hat{\mathbf{z}}$, with interactions dictating the distribution of such orbits (and hence the ODF) in the semidilute regime [M. Rahnama, D. L. Koch, and E. S. G. Shaqfeh, Phys. Fluids **7**, 487 (1995)]. The full ODF can exhibit

anisotropy in the *y-z* plane, but our measurements are insensitive to this.
[18] N. J. Wagner, G. G. Fuller, and W. B. Russel, J. Chem. Phys. **89**, 1580 (1988).
[19] D. Kim, C. D. Han, and P. T. Mather, Macromolecules **33**, 7922 (2000).
[20] E. K. Hobbie, J. Chem. Phys. **121**, 1029 (2004). Note that Eqs. (37)–(40) of this reference contain an error, which is corrected in Eqs. (5) and (6) here.
[21] E. K. Hobbie, H. Wang, H. Kim, C. C. Han, E. A. Grulke, and J. Obrzut, Rev. Sci. Instrum. **74**, 1244 (2003).
[22] Z. M. Li, Z. K. Tang, H. J. Liu *et al.*, Phys. Rev. Lett. **87**, 127401 (2001).
[23] A. Jorio, M. A. Pimenta, A. G. Souza Filho *et al.*, Phys. Rev. Lett. **90**, 107403 (2003).
[24] X. Liu, T. Pichler, M. Knupfer, M. S. Golden, J. Fink, H. Kataura, and Y. Adriba, Phys. Rev. B **66**, 045411 (2002).
[25] P. J. Harris, *Carbon Nanotubes and Related Structures* (Cambridge University Press, Cambridge, 1999).
[26] R. Saito, G. Dresselhaus, and M. S. Dresselhaus, *Physical Properties of Carbon Nanotubes* (Imperial College Press, London, 2003).
[27] D. Fry, B. Langhorst, H. Kim, E. Grulke, H. Wang, and E. K. Hobbie, Phys. Rev. Lett. **95**, 038304 (2005).
[28] M. Doi and S. F. Edwards, *The Theory of Polymer Dynamics* (Oxford University Press, New York, 1986).
[29] D. L. Koch, Phys. Fluids **7**, 2086 (1995).
[30] J. G. Kirkwood and R. J. Plock, J. Chem. Phys. **24**, 665 (1946); G. K. Batchelor, J. Fluid Mech. **41**, 545 (1970).
[31] M. F. Yu, O. Lourie, M. J. Dyer, K. Moloni, T. F. Kelly, and R. S. Ruoff, Science **287**, 637 (2000).
[32] C. F. Schmid and D. J. Klingenberg, Phys. Rev. Lett. **84**, 290 (2000); C. F. Schmid, L. H. Switzer, and D. J. Klingenberg, J. Rheol. **44**, 781 (2000).
[33] Y. Iso, C. Cohen, and D. L. Koch, J. Non-Newtonian Fluid Mech. **62**, 135 (1996).
[34] R. R. Sundararajakumar and D. L. Koch, J. Non-Newtonian Fluid Mech. **73**, 205 (1997).
[35] X. Fan, N. Phan-Thien, and R. Zheng, J. Non-Newtonian Fluid Mech. **74**, 113 (1998).
[36] P. D. Cobb and J. E. Butler, J. Chem. Phys. **123**, 054908 (2005).